# Iterative Learning Control for Compliant Underactuated Arms

Michele Pierallini[1,2], Franco Angelini[1,2], Riccardo Mengacci[1,2], Alessandro Palleschi[1,2], Antonio Bicchi[1,2,3], and Manolo Garabini[1,2]

***Abstract*—Operations involving safe interactions in unstructured environments require robots with adapting behaviors. Compliant manipulators are a promising technology to achieve this goal. Despite that, some classical control problems such as following a trajectory are still open. A typical solution is to compensate the system dynamics with feedback loops. However, this solution increases the effective robot stiffness and jeopardizes the safety property provided by the compliant design. On the other hand, purely feedforward approaches can achieve good tracking performance while preserving the robot intrinsic compliance. However, a feedforward control framework for robots with passive elastic joints is still missing. This article presents an iterative learning control algorithm for purely feedforward trajectory tracking for compliant underactuated arms. Each arm is composed of active elastic joints and a generic number of passive ones connected through rigid links. We prove the convergence of the iterative method, also in the presence of uncertainties and bounded disturbances. Different output functions are analyzed providing conditions, based on the system inertial properties that ensure the algorithm applicability. Additionally, an automatic selection of the learning gain is proposed. Finally, we extensively validate the theoretical results with simulations and experiments.**

***Index Terms*—Robotics, Iterative Learning Control (ILC), flexible structures.**

## I. Introduction

Recent years have seen the growing interest in a novel generation of robots, the so-called soft robots [1]. These systems present lumped elastic elements at the joints [2], flexible elements [3], or continuum soft bodies [4]. We here focus on underactuated compliant arms (Fig. 1), which are soft robots with elastic elements lumped at the joints, and a limited number of actuated joints, leading to a flexible behavior. The elastic elements in soft robots enable a compliant behavior, which is a crucial feature to safely and resiliently interact with unstructured environments, with human beings, and other robots. Additionally, they present properties such as adaptability [5], energy efficiency [6], shock absorption [7], which allow outperforming traditional rigid robots in novel applications such as agri-food [8], healthcare [9], service [10], search & rescue [11], etc.

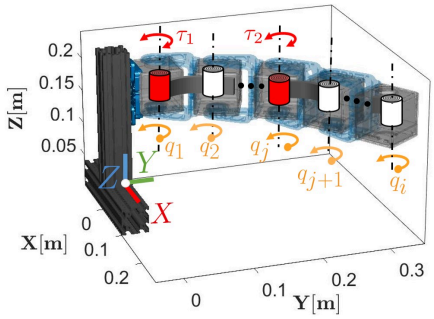


Fig. 1. An underactuated compliant arm is a robot composed of several joints, of which only a few are actuated. The compliance is conferred to the arm by elastic elements lumped at the joints (both actuated and unactuated). It is worth noting that there is no limit on the number of unactuated joints. As an example, the figure depicts a robot with only two actuated elastic joints (red cylinders) and a generic number of passive ones (white cylinders).

With the advent of soft robotics, the control problem radically changed, and several old challenges needed to be reopened, re-analyzed, and solved. Trajectory tracking is one of these classical problems. Historically, robot control was based on the stiffer the better paradigm [12] because robots used to work isolated in cages solving pick and place tasks. Indeed, stiff behavior allows maximizing the robot accuracy [13]. Therefore, controllers mainly incorporated compensation of the robot dynamics [14], and a high-gain feedback-loop [15].

Nowadays, to achieve adaptability and interaction safety, controllers aim to fully exploit the softness of the robot structure. This idea has been implemented into a model-based paradigm [3], [16]–[22] and a learning-based algorithm [23]–[26]. The performance of the former is intrinsically linked to the model accuracy. This may lead to a lack of reliability because the dynamic of soft robots is typically hard-to-model [27]. For this reason, model-based controllers usually present a feedback loop to increase robustness to model uncertainties. However, using a feedback loop will stiffen up the robot behavior [23]. Conversely, feedforward approaches preserve the natural compliance of the robot. For this reason, learning-based methods are a proper solution. Indeed, they mainly rely on feedforward components, and they do not require an accurate description of the robot model. However, machine learning approaches, e.g., Reinforcement Learning [25], are time-consuming, and they do not exploit the system properties,

This research has received funding partially from the European Union's Horizon 2020 Research and Innovation Programme under Grant Agreement No. 101016970 (Natural Intelligence), No. 101017274 (DARKO), in part by Ministry of University and Research (MUR) as part of the PON 2014-2021 "Research and Innovation" resources – Green/Innovation Action - DM MUR 1062/2021, and in part by th Italian Ministry of Education and Research (MIUR) in the framework of the FoReLab project (Departments of Excellence).

[1]Centro di Ricerca "Enrico Piaggio", Università di Pisa Largo Lucio Lazzarino 1, 56126 Pisa, Italy.

[2]Dipartimento di Ingegneria dell'Informazione, Università di Pisa, Largo Lucio Lazzarino 1, 56126 Pisa, Italy

[3]Soft Robotics for Human Cooperation and Rehabilitation, Fondazione Istituto Italiano di Tecnologia, via Morego, 30, 16163 Genova, Italy

michele.pierallini@gmail.com

e.g., inertial coupling [28] or stability [29], [30]. On the other hand, the Iterative Learning Control (ILC) [31] framework consists of an almost purely feedforward iterative control approach that can lead to good tracking performance without requiring an accurate description of the model. ILC has been already applied to robots with elasticity lumped at the joints, and it has been proved to avoid any alteration of the robot compliant dynamics [23], [32]. In [23], ILC deals with robots whose joints are all independently actuated. This control framework is generalized w.r.t. the desired stiffness profile in [24]. However, controlling robots with a generic number of unactuated elastic joints is still an open problem.

In our previous work [33], we proposed an ILC framework that targets the trajectory tracking problem for compliant arms composed of two elastic joints, where only the first is actuated. The main limitations of [33] are that only one unactuated elastic joint is present, only one output function is employed, and only Single-Input Single-Output (SISO) systems are analyzed.

The contributions of the paper are:

1) we propose a pure feedforward ILC law for trajectory tracking for compliant underactuated arms.
   a) The proposed algorithm generalizes [23], [24], [33], [34] managing a generic number of actuated and unactuated elastic joints. This includes also the case of a number of unactuated joints that is even greater than the number of actuated ones (Fig. I). Note also that this algorithm can be applied to Multiple-Input Multiple-Output (MIMO) systems too.
   b) We quantify the robustness of the convergence of the proposed method in the case of continuous time nonlinear systems with a fixed generic relative degree affected by nonrepetitive disturbance. A similar problem is studied in [35]–[37] for discrete-time systems without any relative degree dependence, in [38] the underactuated continuous-time nonlinear system has a relative degree equal to one and saturated iterative control law is employed, and in [39] the nonlinear system is not affected by disturbances. Moreover, these articles do not present any experimental validation.
2) We analyze different choices of the output functions. The main challenge, to guarantee the learning converge, is given by the relative degree dependence [40]. Hence:
   a) we design conditions to ensure the applicability of the learning method, generalizing the Strong Inertial Coupling (SIC) condition [28].
   b) We develop two automatic procedures to select the learning gains while guaranteeing the convergence.
3) We extensively validate the effectiveness of the proposed method through different tests. First, we perform a simulative comparison between the proposed approach and State-of-the-Art (SoA) controllers on a 2 degree of freedoms (DOFs) robot. Second, we validate the proposed method in both simulations and on real hardware. We simulate two systems: a 10 DOFs SISO system, and a 6 DOFs MIMO arm. The former validates the tracking performance of a chain with 9 passive joints and the latter operates in a tridimensional workspace. Then, we compare the results of simulations and experiments for a 2 DOFs chain, a 3 DOFs arm, and a 4 DOFs planar MIMO robot, varying output functions, disturbances, payloads, desired trajectories, and the stiffness values of the joints.

This paper is organized as follows. Sec. II introduces the underactuated compliant arm model, and it defines the control problem. In Sec. III, the design of the ILC is defined. Sec. III-A provides sufficient conditions to guarantee the convergence of the learning based on the inertial coupling property. Sec. III-B derives conditions to ensure the strong inertial coupling considering different output functions, and Sec. III-C proposes two automatic procedures to compute the control gains. Sec. III-D studies the applicability of the learning method, and Sec. IV validates its effectiveness. The results are discussed in Sec. V. Finally, Sec VI reports the conclusions. All the proofs are reported in the Appendix.

## II. Problem Statement

*Notation:* Let $1_{1\times n} = [1, 1, \cdots, 1] \in \mathbb{R}^{1\times n}$, $I_n \in \mathbb{R}^{n\times n}$ be the identity matrix, and $0_n \in \mathbb{R}^{n\times n}$ be a zero matrix. Let $f, g : x \in \mathbb{R}^n \to \mathbb{R}^n$ be two vector fields, $L_f g(x)$ stands for the Lie derivative of $g(x)$ along $f(x)$, i.e., $L_f g(x) = \frac{\partial g(x)}{\partial x} f(x)$. For any matrix $A \in \mathbb{R}^{n\times m}$, we denote with $A_{i,j}$ its $(i,j)-$th element. For any vector $v \in \mathbb{R}^n$, for any matrix $A \in \mathbb{R}^{n\times m}$, we denote with $||v||$ and $||A||$ their infinity norm. Let $\lambda$ be a positive constant, for any vector $v \in \mathbb{R}^n$, we denote with $||v||_\lambda$ its $\lambda-$norm, i.e., $||v||_\lambda \triangleq \sup_t \left\{||v|| \mathrm{e}^{-\lambda t}\right\}$. Finally, let $y(\cdot) : t \in \mathbb{R} \to \mathbb{R}^n$ be a vector function, we denote with $y^{(i)}(t)$ its $i-$th time derivative.

We refer to the model of an $n$-DOFs compliant robot having a combination of actuated and unactuated elastic joints, i.e.,

$$M(q)\ddot{q} + C(q,\dot{q})\dot{q} + G(q) + D\dot{q} + Kq = S\tau + \tau_{\text{ext}} , \quad (1)$$

where $q, \dot{q}, \ddot{q} \in \mathbb{R}^n$ are the joint position, velocity, and acceleration vectors, respectively. $M(q) \in \mathbb{R}^{n\times n}$ is the inertia robot matrix, $C(q,\dot{q}) \in \mathbb{R}^{n\times n}$ is the Coriolis matrix, $G(q) \in \mathbb{R}^n$ is the gravitational term, $D \in \mathbb{R}^{n\times n}$ and $K \in \mathbb{R}^{n\times n}$ are the damping and stiffness matrices, respectively. We indicate with $\tau \in \mathbb{R}^{n_\text{a}}$ the control input, where $n_\text{a}$ indicates the number of active joints. The matrix $S \in \mathbb{R}^{n\times n_\text{a}}$ is the underactuation map, and it is such that $\text{rank}\{S\} = n_\text{a}$. The vector $\tau_{\text{ext}} \in \mathbb{R}^n$ denotes the external disturbances (if present).

We study an iterative procedure over a finite time interval $[0, t_\text{f}]$. Let $j = 0, 1, \cdots$ be the iteration index, we follow the classic affine state-space form representation by defining the state vector $x_j \triangleq \left[q_j^\top,\ \dot{q}_j^\top\right]^\top \in \mathbb{R}^{2n}$ at the $j-$th iteration. Thus, the system (1) can be written as

$$\begin{cases} \dot{x}_j(t) = f(x_j(t)) + g(x_j(t))u_j(t) + v_j(t) & (2) \\ y_j(t) = h(x_j(t)) + w_j(t) , & (3) \end{cases}$$

where $y_j \in \mathbb{R}^{n_\text{y}}$ is the output, $h(\cdot) : \mathbb{R}^{2n} \times [0, t_\text{f}] \to \mathbb{R}^{n_\text{y}}$ is the output function, while $u_j \in \mathbb{R}^{n_\text{a}}$ is the control action, i.e., $\tau$. $f(\cdot) : \mathbb{R}^{2n} \times [0, t_\text{f}] \to \mathbb{R}^{2n}$, and $g(\cdot) : \mathbb{R}^{2n} \times [0, t_\text{f}] \to \mathbb{R}^{2n\times n_\text{a}}$ are the drift and control vector field, respectively, i.e.,

$$f(x_j) = \begin{bmatrix} \dot{q}_j \\ -M^{-1}(q_j)N(q_j,\dot{q}_j) \end{bmatrix},\ g(x_j) = \begin{bmatrix} 0_{n\times n_\text{a}} \\ M^{-1}(q_j)S \end{bmatrix}, \quad (4)$$

with $N(q_j,\dot{q}_j) \triangleq C(q_j,\dot{q}_j)\dot{q}_j + G(q_j) + Kq_j + D\dot{q}_j$.

The nonrepetitive disturbances are $v_j(t) : [0,t_\mathrm{f}] \to \mathbb{R}^{2n}$, which is a more general form of $M^{-1}(q_j)\tau_{\mathrm{ext}_j}(t)$, and $w_j(t) : [0,t_\mathrm{f}] \to \mathbb{R}^{n_\mathrm{y}}$. Moreover, the initial condition $x_j(0) \in \mathbb{R}^{2n}$ presents nonrepetitive bounded deviation from an iteration-constant value $\bar{x}(0) \in \mathbb{R}^{2n}$ such that $x_j(0) = \bar{x}(0) + l_j$, $l_j \in \mathbb{R}^{2n}$.

We assume that

A1) the system (2)-(3) is square, i.e., $n_\mathrm{y} = n_\mathrm{a}$ [39].

A2) The system (2)-(3) has a (vector) relative degree (see, e.g., [40]) $r_\mathrm{v} = [r_1, \ldots, r_{n_\mathrm{a}}]^\top, \forall t \in [0,t_\mathrm{f}]$, with $r_1 = \cdots = r_{n_\mathrm{a}} = r > 0$, for almost all $x \in \mathbb{R}^{2n}$.

It is instrumental for the description of the method to recall the decoupling matrix $E(x) \in \mathbb{R}^{n_\mathrm{a}\times n_\mathrm{a}}$, i.e., $E_{i,k}(x) = L_{g_i}L^{r_k-1}h_k(x)$, with $\forall i,k \in [1,n_\mathrm{a}]$ (see, e.g., [40]).

A3) $f(x)$, $g(x)$, $h(x)$, $L_f^s h(x)$, $s = 1,\cdots,r$, and $E(x)$ are globally Lipschitz with constants $f_0$, $g_0$, $h_0$, $\Phi_s$, and $\eta \in \mathbb{R}$, respectively.

**Remark 1.** *Assumptions A1-A3 are commonly used in the ILC framework [35], [39]. In particular, assumption A1 prevents dimensional ambiguity while inverting the decoupling matrices. Note that assumption A1 does not limit the choice of the output function but only its dimension. This means that both actuated and unactuated variables can be included in* (3)*. Assumption A2 allows a dynamic coupling between the output time derivatives and the control inputs. The Lipschitz assumption, i.e. A3, implies that the functions in* (2)-(3) *and their Lie derivatives are continuous in x.*

Given the desired output trajectory $y_\mathrm{d}(t) : [0,t_\mathrm{f}] \to \mathbb{R}^{n_\mathrm{a}}$, we introduce the definition of realizable reference [38], [39].

**Definition 1.** *The desired trajectory* $y_\mathrm{d}(t) : [0,t_\mathrm{f}] \to \mathbb{R}^{n_a}$ *is said realizable when there exists the unique desired control action* $u_\mathrm{d} \in \mathbb{R}^{n_\mathrm{a}}$ *and a desired state* $x_\mathrm{d} \in \mathbb{R}^{2n}$ *such that* $\dot{x}_\mathrm{d}(t) = f(x_\mathrm{d}(t)) + g(x_\mathrm{d}(t))u_\mathrm{d}(t)$ *and* $y_\mathrm{d} = h(x_\mathrm{d}(t))$.

Given the desired output, which is feasible, continuous, and differentiable for, at least, $r$ times, $\forall t \in [0,t_\mathrm{f}]$, the goal of this work is to design a control input for a system affected by disturbances in the form (2)-(3) under assumptions A1-A3, able to follow the desired trajectory $y_\mathrm{d}$ with a bounded error in $\lambda-$norm. Additionally, to preserve the intrinsic compliance of the system, the control action must be feedforward [32].

## III. Solution

In this section, the problem defined in Sec. II is tackled. We design an ILC controller [31], [39], we prove its convergence and study its robustness to disturbances and uncertainties (Theorem 1). To ensure the method convergence, we investigate the system inertial coupling property for different choices of the output function (Proposition 1). Corollary 2 and 3 present two automatic procedures to select the learning gains. Finally, we studies the method applicability w.r.t. the robot design.

### A. Control Design

Through trails of the same task, the ILC learns a feedforward action that is able to drive the robot following the desired trajectory $y_\mathrm{d}$, while preserving the system elasticity.

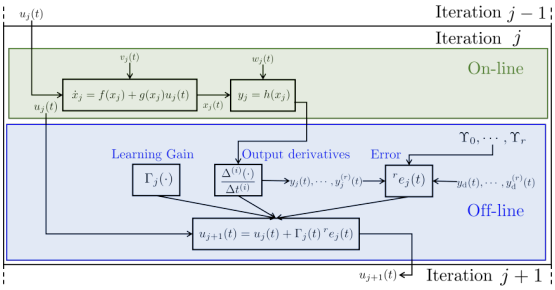


Fig. 2. Scheme of a single iteration of the proposed ILC approach. The "On-line" green box shows the trial execution. The "Off-line" blue box shows the computation of the control action for the next iteration.

Recalling the system (2)-(3) and the assumptions A1-A3, we define the pure feedforward control law as

$$u_{j+1}(t) = u_j(t) + \Gamma_j(t)\,{}^r e_j(t)\,, \tag{5}$$

where $\Gamma_j(t) \in \mathbb{R}^{n_\mathrm{a}\times n_\mathrm{a}}$ is a learning gain which is both time and iteration variant, and the error is defined as

$$\begin{aligned} {}^r e_j(t) &\triangleq \sum_{s=0}^{r} \Upsilon_s \left(L_f^s h(x_\mathrm{d}) - L_f^s h(x_j)\right) \\ &\quad + \Upsilon_r \left(E(x_\mathrm{d})u_\mathrm{d} - E(x_j)u_j\right) - \sum_{s=0}^{r} \Upsilon_s w_j^{(s)} \\ &= \Phi(x_j,x_\mathrm{d}) + \Upsilon_r \left(E(x_\mathrm{d})u_\mathrm{d} - E(x_j)u_j\right) - \sum_{s=0}^{r} \Upsilon_s w_j^{(s)}\,, \end{aligned} \tag{6}$$

where $E(x) \in \mathbb{R}^{n_\mathrm{a}\times n_\mathrm{a}}$ is the decoupling matrix, and $\Upsilon_s \in \mathbb{R}^{n_\mathrm{a}\times n_\mathrm{a}}$, $\Upsilon_s \succ 0$, $s = 0,\ldots,r$ are the control gains. The controller (5) requires an *initial guess* $u_0$, which can be freely chosen. Fig. 2 shows the block-diagram of the proposed approach.

Def. 1 provides the existence of $u_\mathrm{d}$ and $x_\mathrm{d}$, which are required to theoretically prove the convergence of (5) (Theorem 1). However, the knowledge of $u_\mathrm{d}$ and $x_\mathrm{d}$ is not required, and from a practical point of view, the controller only needs the output and its time derivatives, i.e., (6).

In the following Theorem, we prove the convergence of the proposed iterative controller (5).

**Theorem 1.** *Let us consider the system* (2)-(3) *under assumptions A1-A3, the control law* (5)*, a desired output* $y_\mathrm{d}(t) \in \mathbb{R}^{n_\mathrm{a}}$*, and the error definition* (6)*. Let us suppose that the nonrepetitive disturbances are bounded, i.e.,* $\sup_j \max_t \left\{\left|\left|v_j(t)\right|\right|\right\} \leq b_\mathrm{v} < +\infty$*,* $\sup_j \max_t \left\{\left|\left|w_j(t)\right|\right|\right\} \leq b_\mathrm{w} < +\infty$*, and let* $\bar{x}(0) = x_\mathrm{d}(0)$ *be such that* $x_j(0) = x_\mathrm{d}(0) + l_j$*, with* $\sup_j \left\{\left|\left|l_j\right|\right|\right\} \leq b_\mathrm{l} < +\infty$*. Moreover, let us suppose that* $w_j(t)$ *can be differentiated r times with bounded derivatives, i.e.,* $\sup_j \max_t \{\left|\left|w_j^{(s)}(t)\right|\right|\} \leq b_\mathrm{ws}$*, where* $b_\mathrm{ws}$ *with* $s = 1,\cdots,r$*.*

*If the learning gain* $\Gamma_j(t) \in \mathbb{R}^{n_\mathrm{a}\times n_\mathrm{a}}$ *satisfies*

$$\left|\left|I_{n_\mathrm{a}} - \Gamma_j(t)\Upsilon_r E(x_j)\right|\right| \leq \rho < 1\,, \forall t \in [0,t_\mathrm{f}]\,, j = 0,1,\ldots\,, \tag{7}$$

*where* $E(x) \in \mathbb{R}^{n_\mathrm{a}\times n_\mathrm{a}}$ *is the decoupling matrix, and* $\Upsilon_r \in \mathbb{R}^{n_\mathrm{a}\times n_\mathrm{a}}$

*is a control gain, then*

$$\lim_{j\to+\infty} \left\|u_{\mathrm{d}}(t)-u_j(t)\right\|_{\lambda} \to b_{\mathrm{u}} \tag{8}$$

$$\lim_{j\to+\infty} \left\|x_{\mathrm{d}}(t)-x_j(t)\right\|_{\lambda} \to b_{\mathrm{x}} \tag{9}$$

$$\lim_{j\to+\infty} \left\|{}^{r}e_j(t)\right\|_{\lambda} \to b_{\mathrm{e}}\,, \tag{10}$$

*where $b_{\mathrm{u}}, b_{\mathrm{x}}$, and $b_{\mathrm{e}}$ are finite positive constants dependent on $b_{\mathrm{l}}$, $b_{\mathrm{v}}$, $b_{\mathrm{w}}$, and $b_{\mathrm{ws}}$ for $s = 1,\cdots,r$.*

*Proof.* See the Appendix. □

**Remark 2.** *The presence of bounded disturbances in Theorem 1 allows to derive robust result on the convergence, i.e.,* (10)*. Note that, since the* (5) *is purely feedforward, we can differentiate the disturbances $w_j(t)$ off-line after filtering gaining bounded derivatives.*

**Corollary 1.** *Suppose that all the hypotheses of Theorem 1 are verified with $l_j = 0$, $v_j(t) = 0$, and $w_j(t) = 0, \forall t \in [0,t_{\mathrm{f}}], \forall j$. If the learning gain $\Gamma_j(t) \in \mathbb{R}^{n_{\mathrm{a}}\times n_{\mathrm{a}}}$ satisfies* (7)*, then the Thesis of Theorem 1 is still valid with $b_{\mathrm{u}} = b_{\mathrm{x}} = b_{\mathrm{e}} = 0$.*

*Proof.* See the Appendix. □

**Remark 3.** *The control algorithm* (5) *is able to manage also repetitive disturbances $d_{\mathrm{d}}(x) : \mathbb{R}^{2n} \to \mathbb{R}^{2n}$ and multiplicative uncertainties $\psi \in \mathbb{R}$. The system* (2) *can be rewritten as $\dot{x}_j = \psi f(x_j) + \psi g(x_j)u_j + d(x_j) + v_j$, thus any repetitive disturbance $d_{\mathrm{d}}(x)$ can be included in the drift field $f(x)$ [31].*

Finally, it is worth noting that assumptions A1 and A2 can be relaxed at the cost of more complex notation. Assumption A1 requires a study of the null space of the decoupling matrix. Results of Theorem 1 can also be obtained considering in assumption A2 that $r_i \neq r_j$, when $i \neq j$, $i,j = 1,\cdots,n_{\mathrm{a}}$. This is beyond the scope of this work and assumption A3 will be analyzed in future work.

### *B. On the Inertial Coupling Property of Compliant Arms*

In Sec. III-A, we proved the convergence of (5) based on the assumption A2, which depends on the chosen output function. In this section, we study how different choices of the desired output function (3) affect the validity of the assumption A2. In particular, we propose dynamic conditions that ensure a fixed relative degree based on the inertial coupling of robot. To keep the notation simple, we will omit the iteration dependency.

**Proposition 1.** *Let us consider a system in the form* (1)-(2)-(3)*, under assumptions A1,A3. Let $h(q,\dot{q}) \in \mathbb{R}^{n_{\mathrm{a}}}$ be the output function, which includes the positions and velocities of the joints, then the relative degree $r$ is $r = 1$ iff*

$$\operatorname{rank}\{E\} = \operatorname{rank}\left\{\frac{\partial h(q,\dot{q})}{\partial \dot{q}} M^{-1}(q) S\right\} = n_{\mathrm{a}}, \forall q,\dot{q} \in \mathbb{R}^n\,, \tag{11}$$

*where $E(x) \in \mathbb{R}^{n_{\mathrm{a}}\times n_{\mathrm{a}}}$ is the decoupling matrix.*

*Conversely, if the output function does not include the velocities, the relative degree $r$ is $r = 2$ iff*

$$\operatorname{rank}\{E\} = \operatorname{rank}\left\{\frac{\partial L_f h(q,\dot{q})}{\partial q} M^{-1}(q) S\right\} = n_{\mathrm{a}}, \forall q,\dot{q} \in \mathbb{R}^n\,. \tag{12}$$

*Proof.* See the Appendix. □

It is worth noting that (11) and (12) depend on the inertial coupling of the system (1) and on the chosen trajectory (3).

**Remark 4.** *Recalling system* (1)-(2)-(3)*, we highlight that* (12)*, is a more general result of the SIC definition [28]. In [28], the output function was the active joint positions vector, namely collocated variables. Conversely,* (12) *can be applied to any output choice. In the case of $y = S_{\mathrm{a}}q$ with $S_{\mathrm{a}} = S^{\top}$,* (12) *becomes* $\operatorname{rank}\left\{S_{\mathrm{a}}M^{-1}(q)S\right\} = n_{\mathrm{a}}$*, [28]. Note that no assumption is required on the number of the passive joints.*

In this work, two output functions are analyzed. Firstly, we focus on the absolute angle of the tip of the robot, i.e.,

$$y = h(x) = 1_{1\times n} q \quad 1_{1\times n} = [1,\cdots,1] \in \mathbb{R}^{1\times n}\,. \tag{13}$$

Secondly, we use the Cartesian Planar position of the robot tip. The chosen output function for planar operations is

$$y = \begin{bmatrix} y_{\mathrm{X}}(q) \\ y_{\mathrm{Y}}(q) \end{bmatrix} \in \mathbb{R}^2 \begin{cases} y_{\mathrm{X}}(q) = \sum_{i=1}^{n} l_{\mathrm{c}_i} \cos(\sum_{j=1}^{i} q_j) \\ y_{\mathrm{Y}}(q) = \sum_{i=1}^{n} l_{\mathrm{c}_i} \sin(\sum_{j=1}^{i} q_j) \end{cases} \tag{14}$$

where $l_{\mathrm{c}_i} \in \mathbb{R}, i = 1,\cdots,n$ is the centre of mass distance of the $i-$th link. Instead, if the robot operates in a tridimensional workspace, we can use the direct kinematics map, i.e.,

$$y = [y_{\mathrm{X}}(q),\ y_{\mathrm{Y}}(q),\ y_{\mathrm{Z}}(q)]^{\top} \in \mathbb{R}^3\,. \tag{15}$$

Note that the output functions (13),(14), and (15) depend on the whole joints' position and in no way the output is limited to include only the position of actuated joints.

### *C. Automatic Gains Selection to Guarantee the Convergence*

In this section, we propose two automatic procedures to design the learning gain $\Gamma_j(t) \in \mathbb{R}^{n_{\mathrm{a}}\times n_{\mathrm{a}}}$ to fulfill (7).

**Corollary 2.** *Under the same assumptions of Proposition 1, let $h(q) \in \mathbb{R}^{n_{\mathrm{a}}}$ be the output function, and let* (12) *be true. If we choose the leaning gain $\Gamma_j(t) \in \mathbb{R}^{n_{\mathrm{a}}\times n_{\mathrm{a}}}$ such as*

$$\Gamma_j(t) = \varepsilon E^{-1}(q_j,\dot{q}_j)\Upsilon_r^{-1}\,,\ \varepsilon \in [0,1),\ \forall t \in [0,t_{\mathrm{f}}], \forall j\,, \tag{16}$$

*where $E(x) \in \mathbb{R}^{n_{\mathrm{a}}\times n_{\mathrm{a}}}$ is the decoupling matrix, and $\Upsilon_r \in \mathbb{R}^{n_{\mathrm{a}}\times n_{\mathrm{a}}}$ is the control gain, then the condition* (7) *in Theorem 1 holds.*

*Proof.* See the Appendix. □

Applying Corollary 2 to the output (13), (16) becomes

$$\Gamma_j(t) = \varepsilon / \left(1_{1\times n} M^{-1}(q_j) S\right)\,. \tag{17}$$

From a practical point of view, a trivial case in which (17) is not fulfilled is $\sum_{i=2}^{n} \nu_i q_i = \pi/2$ where $\nu_i \in \mathbb{R}, i = 2,\cdots,n$. Hence, the angle between the tip of the robot and the first link position $q_1$ is equal to $\pi/2$. Corollary 2 is an automatic procedure, which allows a precise design of the learning gains $\Gamma_j(t)$ in (7). However, it presents two limitations. First, it requires the full knowledge of the inertia matrix of the robot. Second, if the relative degree changes, (16) is divergent. Therefore, we propose an alternative gain selection method.

**Corollary 3.** *Under the same assumptions of Proposition 1 and A2, let $h(x) \in \mathbb{R}^{n_{\mathrm{a}}}$ be the output function, and let $\omega$ be*

*a finite constant value such as* $\omega \gg \max_t ||\Upsilon_r E(x(t))||$. *If we choose a time and iteration constant learning gain* $\Gamma$ *such as*

$$\Gamma_{i,i} = \text{sgn}\Big\{ \sum_{j=1}^{n_\text{a}} E_{i,j} \Big\} / \omega \,, \quad i = 1, \cdots, n_\text{a} \,, \tag{18}$$

*where* $\Gamma_{i,i}$ *is the* $i-$*th diagonal element of* $\Gamma \in \mathbb{R}^{n_\text{a} \times n_\text{a}}$, *and* $E(x) \in \mathbb{R}^{n_\text{a} \times n_\text{a}}$ *is the decoupling matrix; then the condition* (7) *in Theorem 1 holds.*

*Proof.* See the Appendix. □

The iterative controller (5) with learning gain (17) requires the knowledge of the robot's inertial model. Conversely, (18) requires the boundedness of the inertia matrix and some information on the sign of decoupling matrix's elements to guarantee the convergence of (5).

### D. Method Applicability

We here study the applicability of the iterative method. As depicted by Fig. 2, (5) is purely feedforward, and it cannot be applied to any unstable system. Hence, we discuss about the open-loop stability of a generic underactuated compliant arm.

Recalling (1) and (4), the stability depends on the drift vector. Thus, it is strictly connected to the stiffness [15], [32], [41]. Let us consider any equilibrium point such as $\overline{x} = \left[\overline{q}^\top, 0_{1\times n}^\top\right]^\top$, we linearize (1) around the pair $(\overline{x}, \overline{u})$, i.e.,

$$\dot{\tilde{x}} = \begin{bmatrix} 0_n & I_n \\ -M^{-1}(q)\left(\frac{\partial G(q)}{\partial q} + K\right)\Big|_{\overline{q}} & -M^{-1}(\overline{q})D \end{bmatrix} \tilde{x} + \begin{bmatrix} 0_{n\times n_\text{a}} \\ M^{-1}(\overline{q})S \end{bmatrix} \tilde{u} \tag{19}$$

where $\tilde{x} \triangleq x - \overline{x}$, and $\tilde{u} \triangleq u - \overline{u}$. Consider (19), if $M^{-1}(q)\left(\partial G(q)/\partial q + K\right)\big|_{\overline{q}} \succ 0$, then the overall matrix is Hurwitz and Lyapunov indirect Theorem implies that (2) is asymptotically stable in $(\overline{x}, \overline{u})$. Since $M^{-1}(q)\left(\partial G(q)/\partial q + K\right)\big|_{\overline{q}}$ depends on the dynamic parameters, e.g., stiffness, design choices can lead to the asymptotic stability of the equilibrium or around trajectories.

Conversely, a feedback controller could stabilize the closed-loop system [15], [42] at the cost of a stiffening of the robot behavior [32], and of the necessity of a novel convergence condition. This problem is out of the scope of this paper.

## IV. Validation

In this section, we validate the effectiveness of the proposed method on compliant arms through simulations and experiments. First, the proposed technique is compared with SoA controllers. Then, we extensively validate the proposed approach on several different robotic structures in different conditions. In the following, we denote with $R$ the active revolute joints and with $\overline{R}$ the passive ones.

### A. Simulation and Experimental Setup

We simulate the five systems, namely $R\overline{R}$ in Fig. 3(a), $R\overline{9}\overline{R}$ in Fig. 3(b), $R\overline{R}R\overline{R}R\overline{R}$ in Fig. 3(c), $R\overline{2}\overline{R}$ in Fig. 3(d), $R\overline{R}R\overline{R}$ in Fig. 3(e), respectively. To simulate the dynamics, we employ the `Robotics System Toolbox` by MATLAB, and the dynamic parameters are reported in Tab. I, where $J$, $m$, $a$, $l_\text{c}$, $k$, and $d$ are the inertia, mass, length, center of mass distance, spring, and damper of each link, respectively. The joint springs and dampers are assumed linear.

We perform simulations to compare ILC with the SoA on the $R\overline{R}$ in Sec. IV-C. We simulate the $R\overline{9}\overline{R}$ in Sec. IV-D, and $R\overline{R}R\overline{R}R\overline{R}$ in Sec. IV-E. Simulations, which are carried out with the $R\overline{R}$, $R\overline{2}\overline{R}$, and $R\overline{R}R\overline{R}$ system, are compared with the experimental results in Sec IV-F, Sec. IV-G, and Sec. IV-H. It is worth noting that $M^{-1}(q)\left(\partial G(q)/\partial q + K\right)\big|_{\overline{q}} \succ 0, \forall \overline{q} \in \mathbb{R}^n$, hence the equilibrium of the system is asymptotically stable, and the controller (5) is applicable.

In the experiments, as elastic actuators, we employ a qbMove Advanced, which are variable stiffness actuators [43]. This actuator is based on the agonistic-antagonistic principle, for which two motors connect the output shaft via a nonlinear elastic mechanism. The actuators are equipped with an AS5045 12 bit magnetic encoder.

The elastic torque $\tau_\text{e}$ and the nonlinear stiffness function $\sigma$ of the actuator are $\tau_\text{e} = 2\beta\cosh(\alpha\theta_\text{s})\sinh(\alpha(q_i - \theta_\text{e}))$ and $\sigma = 2\alpha\beta\cosh(\alpha\theta_\text{s})\cosh(\alpha(q_i - \theta_\text{e}))$, where $\alpha = 6.7328\text{rad}^{-1}$, $\beta = 0.0222\text{Nm}$, and $q_i$ is the Lagrangian variable of the $i-$th active link $i = 1, \cdots, n_\text{a}$. This actuator can be controlled through two parameters $\theta_\text{s}$ and $\theta_\text{e}$. $\theta_\text{s}$ tunes the desired stiffness profile and will be set constant. Note that this leads to a nonlinear stiffness profile, differently from the stiffness matrix $K$ in (1). $\theta_\text{e}$ is the motor equilibrium position, and, assuming a negligible motor dynamics, it becomes the control input $\tau$ in (1) by multiplying it for the joint stiffness.

To implement a passive joint, we employ a qbMove Advanced actuator, where $\theta_\text{s}$ is set constant, while $\theta_\text{e}$ is set null. Thanks to this practical method, we have a passive joint with a torsional spring and a position encoder sensor.

### B. Simulation and Experimental Description

We first compare the proposed method with SoA controllers in simulation on the SISO $R\overline{R}$ system in Fig 3(a). Then, the proposed technique is validated through several simulations and experiments on systems depicted in Fig 3 varying payload masses, stiffness profiles, nonrepetitive disturbances, trajectories, and output functions. For the SISO systems, namely

TABLE I
DYNAMIC MODEL PARAMETERS.

$R\overline{R}$

| Link | $m$[kg] | $l_\text{c}$[m] | $a$[m] | $J$[kgm$^2$] | $k\left[\frac{Nm}{\text{rad}}\right]$ | $d\left[\frac{\text{Nms}}{\text{rad}}\right]$ |
|---|---|---|---|---|---|---|
| 1 | 0.55 | 0.085 | 0.089 | 0.002 | 3,5.04 | 0.3 |
| 2 | 0.45,0.15 | 0.085 | 0.089 | 0.002,9e−4 | 3,5.04 | 0.3 |

$R\overline{9}\overline{R}$

| Link | $m$[kg] | $l_\text{c}$[m] | $a$[m] | $J$[kgm$^2$] | $k\left[\frac{Nm}{\text{rad}}\right]$ | $d\left[\frac{\text{Nms}}{\text{rad}}\right]$ |
|---|---|---|---|---|---|---|
| $1,\cdots,9$ | 0.085 | 0.085 | 0.089 | 7e−4 | 5.04 | 0.3 |
| 10 | 0.02 | 0.085 | 0.089 | 6e−4 | 5.04 | 0.3 |

$R\overline{2}\overline{R}$

| Link | $m$[kg] | $l_\text{c}$[m] | $a$[m] | $J$[kgm$^2$] | $k\left[\frac{Nm}{\text{rad}}\right]$ | $d\left[\frac{\text{Nms}}{\text{rad}}\right]$ |
|---|---|---|---|---|---|---|
| 1,2 | 0.25 | 0.085 | 0.089 | 0.001 | 3,5.04 | 0.3 |
| 3 | 0.20 | 0.085 | 0.089 | 0.001 | 3,5.04 | 0.3 |

$R\overline{R}R\overline{R}$, and $R\overline{R}R\overline{R}R\overline{R}$

| Link | $m$[kg] | $l_\text{c}$[m] | $a$[m] | $J$[kgm$^2$] | $k\left[\frac{Nm}{\text{rad}}\right]$ | $d\left[\frac{\text{Nms}}{\text{rad}}\right]$ |
|---|---|---|---|---|---|---|
| $1,\cdots,6$ | 0.55 | 0.085 | 0.089 | 0.001 | 5.04 | 0.3 |

$R\overline{R}$, $R\overline{9}\overline{R}$, and $R\overline{2}\overline{R}$, the chosen output function is (13) and

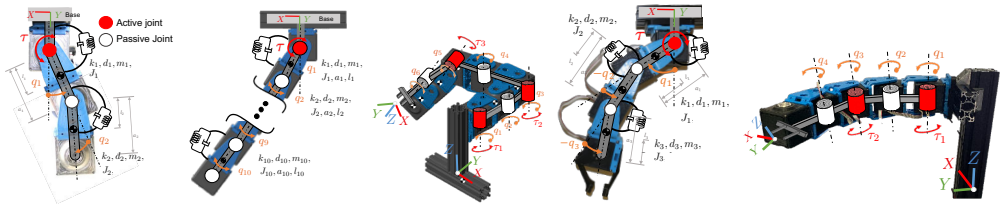


(a) $R\overline{R}$ System. (b) $R\overline{9}\overline{R}$ System. (c) $R\overline{R}R\overline{R}R\overline{R}$ System. (d) $R\overline{2}\overline{R}$ System. (e) $R\overline{R}R\overline{R}$ System.

Fig. 3. Pictures of the compliant robots employed as simulation and experimental testbed. (a), (b), (d) are SISO systems, while (c) and (e) are MIMO. In (b) and (c) are reported the simulated models. (a), (d), and (e) depict the 2 DOFs, 3 DOFs, and 4 DOFs arm employed in the experiments, respectively.

as reference trajectory $y_\mathrm{d}$ we use two trajectories. First, a sinusoidal signal lasting for $t_\mathrm{f} = 6$s, i.e.,

$$y_\mathrm{d}(t) = \pi/8 \cos(t+\pi) + \pi/8 \,. \tag{20}$$

Second, a minimum jerk signal that starts from $y_\mathrm{s}$ and reaches $y_\mathrm{f} = \frac{\pi}{4}$ in $t_\mathrm{f} = 10$s or 1s, i.e., defining $t_\mathrm{t} \triangleq t/t_\mathrm{f}$, one has

$$y_\mathrm{d}(t) = y_\mathrm{f} + (y_\mathrm{f} - y_\mathrm{s}) \left(10t_\mathrm{t}^3 - 15t_\mathrm{t}^4 + 6t_\mathrm{t}^5\right) \,. \tag{21}$$

Conversely, for the MIMO systems, namely $R\overline{R}R\overline{R}R\overline{R}$ and $R\overline{R}R\overline{R}$, we choose (14) and (15) performing a minimum jerk trajectory (21). Additionally, with the $R\overline{R}R\overline{R}$ system, we perform also a planar circumference, i.e., defining $\iota \triangleq 2\pi t_\mathrm{t} - \pi$

$$y_{\mathrm{d}_X}(t) = y_\mathrm{X}(0) + r_\mathrm{c}\cos(\iota)\,, \quad y_{\mathrm{d}_Y}(t) = y_\mathrm{Y}(0) + r_\mathrm{c}\sin(\iota)\,, \tag{22}$$

where $r_\mathrm{c}$ is the radius, $t_\mathrm{t} = t/t_\mathrm{f}$ with $t_\mathrm{f}$ final time, and $y(0) = y(t_\mathrm{f}) = [y_\mathrm{X}(0),\ y_\mathrm{Y}(0)]^\top$ is the Cartesian initial and final position of the tip of the robot.

The dynamic model, described in Sec. IV-A, is used both for simulating the system and for tuning the learning gain $\Gamma_j(t)$ of the controller (5) in the experimental trials.

To fulfill the convergence condition (7) in Theorem 1, we employ one of the two gain selection methods proposed in Sec. III-C: Gain Selection Procedure 1 (namely, GSP1), i.e., (16) in Corollary 2, or Gain Selection Procedure 2 (namely, GSP2), i.e., (18) in Corollary 3. In (16), we set the parameter $\varepsilon$ as $\varepsilon = 0.9$. The value of the control gains $\Upsilon_i$, $i = 0, \cdots, r$ is chosen depending on the test: Tab. II lists the control parameters $\Upsilon_0, \Upsilon_1, \Upsilon_2$ used in each simulation and experiment.

The initial guess $u_0 \in \mathbb{R}^{n_\mathrm{a}}$ is the constant input able to maintain the robot in the starting configuration $\bar{x}(0) = \left[\overline{q}^\top(0),\ 0_{1\times n}\right]^\top \in \mathbb{R}^{2n}$, i.e., solving $Su_0(t) = G(\overline{q}(0)) + K\overline{q}(0)$. It is worth noting that the nonrepetitive disturbances $l_j$ in the experiments are such that $l_j \neq 0_{2n\times 1}, \forall j$.

We utilize the root mean square (RMS) error as a metric to evaluate the controller tracking performance. As a result, for MIMO systems, the error is calculated as the RMS error of each output function Euclidean norm.

Note that the controller (5) requires up to the $r-$th order differentiation of the output signal. Thanks to the feedforward nature of the controller, the estimation of the output derivatives is performed off-line using the the numerical gradient.

Finally, we highlight that the main discrepancies between simulations and experiments are due to the inaccurate dynamic model, output derivative estimate, and nonlinear joint stiffness.

TABLE II
SIMULATIONS AND EXPERIMENTS CONTROL GAINS
SISO: $[\upsilon_0, \upsilon_1, \upsilon_2]$ , MIMO: $[\upsilon_0 I_{n_\mathrm{a}}, \upsilon_1 I_{n_\mathrm{a}}, \upsilon_2 I_{n_\mathrm{a}}]$

| $R\overline{R}$ | **Sim.** | Sin. | Min. Jerk 10s | Min. Jerk 1s |
|---|---|---|---|---|
| | Heavy, Light | $[250,10,1]$ | $[250,10,1]$ | $[250,10,1]$ |
| | **Exp.** | Sin. | Min. Jerk 10s | Min. Jerk 1s |
| | Heavy | $[200,0.5,0.5]$ | $[250,0.5,0.5]$ | $[250,0.5,0.5]$ |
| | Light | $[150,5,0.3]$ | $[250,5,0.3]$ | $[250,5,0.3]$ |

| $R\overline{9}\overline{R}$ | **Sim.** | Sin. | Min. Jerk |
|---|---|---|---|
| | $\theta_\mathrm{s} = 0.523$ | $[1,0.1,0.01]$ | $[1,0.1,0.01]$ |
| $R\overline{R}R\overline{R}R\overline{R}$ | **Sim.** | Swing | |
| | $\theta_\mathrm{s} = 0.523$ | $[20,1,0.1]$ | |
| $R\overline{2}\overline{R}$ | **Sim.** | Sin. | Min. Jerk 10s |
| | $\theta_\mathrm{s} = 0.523, 0.349$ | $[80,1,1]$ | $[80,1,1]$ |
| | **Exp.** | Sin. | Min. Jerk 10s |
| | $\theta_\mathrm{s} = 0.523, 0.349$ | $[150,1,1]$ | $[150,1,1]$ |
| $R\overline{R}R\overline{R}$ | **Sim.** | Circ. | Swing |
| | $\theta_\mathrm{s} = 0.523, 0.349$ | $[50,5,1]$ | $[50,5,1]$ |
| | **Exp.** | Circ. | Swing |
| | $\theta_\mathrm{s} = 0.523, 0.349$ | $[20,1,0.1]$ | $[20,1,0.1]$ |

### C. Simulation Results: SoA and ILC Comparison on $R\overline{R}$

This section compares the proposed method with SoA controllers simulating the $R\overline{R}$ system described in Tab. I, with $S = [1,0]^\top$, $n = 2$, and $n_\mathrm{a} = 1$. More details about the $R\overline{R}$ system can be found in [33].

We implement two baseline controllers: a Proportional-Derivative (PD) [15] and a Computed Torque (CT) [44]. The former is model-free, and its control law can be written as

$$\tau(t) = K_\mathrm{V}\left(\dot{y}_\mathrm{d}(t) - \dot{y}(t)\right) + K_\mathrm{P}\left(y_\mathrm{d}(t) - y(t)\right) \,, \tag{23}$$

where $K_\mathrm{V} = 1$ and $K_\mathrm{P} = 10$. The CT method is model-based. Recalling (1), the CT control law can is

$$\begin{aligned}\tau(t) = &\left(M_{1,1}(q) - M_{1,2}(q)M_{22}^{-1}M_{2,1}(q)\right)\hat{u}(t) \\ &+ N_1(q,\dot{q}) - M_{1,2}(q)M_{2,2}^{-1}N_2(q,\dot{q})\,,\end{aligned} \tag{24}$$

where $\hat{u} \in \mathbb{R}$ is a PD action such as (23). These two methods are compared with the proposed ILC, whose learning gain is designed via GSP1. The starting configuration is $\bar{x}_0 = 0_{4\times 1}$, thus the ILC initial guess $u_0 \in \mathbb{R}$ is equal to zero.

We apply all controllers to the minimum jerk reference (21). We test both the case of perfect knowledge of the model parameters (Tab.I), and the case of an inaccurate model. The latter is obtained introducing a multiplicative uncertainty on the masses and inertias in Tab.I, i.e., $\tilde{m}_i = 0.9m_i, \tilde{J}_i = 0.9J_i$, $i = 1,2$. This case will be referred to as Perturbed and, we do not test the PD Perturbed case because it is completely model-free.

Fig. 4 compares results with all controllers in all scenarios. Fig. 4(a), reports the error evolution, while Fig. 4(b) shows the final output evolution.

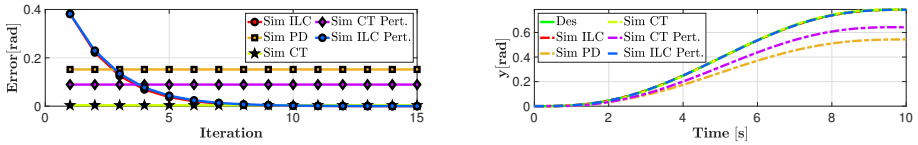


(a) Error evolution. (b) Output evolution .

Fig. 4. $R\overline{R}$: simulation results for the minimum jerk trajectory. Different control actions have been tested by varying the parameters.

### D. Simulation Results: $R\overline{9}\overline{R}$

We here report the results of the $R\overline{9}\overline{R}$ system, whose dynamic parameters are listed in Tab. I, with $S = \left[1, 0_{9\times1}^{\top}\right]^{\top}$, $n = 10$, and $n_{\mathrm{a}} = 1$. This simulation aims at testing the performance of the proposed method in presence of nine passive joints. Furthermore, we compare the performance of GSP1 and GSP2. This is done both with and without disturbances. Indeed, we also inject Gaussian noise with zero mean and standard deviation $10^{-3}$ and $10^{-4}$ in the position and velocities measurements, respectively. The output function is (13), the starting configuration is $\bar{x}(0) = 0_{20\times1}$ thus, the initial guess $u_0 \in \mathbb{R}$ is equal to zero.

Fig. 5 reports the results for (20) and (21). Fig. 5(a) and 5(c) show the error evolution, while Fig. 5(b) and 5(d) report the final output evolution.

### E. Simulation Results: $R\overline{R}R\overline{R}\overline{R}$

We here report the results of the $R\overline{R}R\overline{R}\overline{R}$ system, whose dynamic parameters are listed in Tab. I. The selection matrix $S \in \mathbb{R}^{n\times n_{\mathrm{a}}}$, with $n = 6$ and $n_{\mathrm{a}} = 3$, is a null matrix except for $S_{1,1} = S_{3,2} = S_{5,3} = 1$. This simulation validates the performance of (5) dealing with MIMO systems moving in the Cartesian space, i.e., the output function is (15). The robot swings from the initial Cartesian position $y_{\mathrm{s}} = y(0) = [0,\ 0.4,\ -0.3]^{\top}$m to the final position $y_{\mathrm{f}} = y(t_{\mathrm{f}}) = [-0.43,\ 0.03,\ 0.03]^{\top}$m. Then, it swings back to the initial one, i.e., $y(2t_{\mathrm{f}}) = y(0)$. The desired trajectory is composed of two minimum jerk signals (21) lasting $t_{\mathrm{f}} = 5$s each, so the task lasts 10s in total. The starting configuration is $\bar{x}(0) = 0_{12\times1}$ thus, the initial guess $u_0 \equiv 0_{3\times1}$. The learning gain is designed via GSP2, i.e., (18).

Fig. 6 reports the results. Fig. 6(a) reports the error evolution. Fig. 6(b) shows the final output evolution in the Cartesian space, formally (15). Fig. 6(c) visualizes the robot motion in the initial, middle, and final configuration. Finally Fig. 6(d) depicts the learned control action.

### F. Simulation and Experimental Results: $R\overline{R}$

This experiment aims at validating the proposed approach varying the mass of the second link of the $R\overline{R}$ system: Light ($m_2 = 0.15$kg), and Heavy payload configuration ($m_2 = 0.55$kg), as reported in Tab. I, with $S = [1, 0]^{\top}$, $n = 2$, and $n_{\mathrm{a}} = 1$. A comparison between simulation and experiment is also presented. The output function is (13) with starting configuration $\bar{x}(0) = 0_{4\times1}$. Consequently, the initial guess $u_0 \in \mathbb{R}$ is equal to zero. The learning gain is designed using GSP1 using the nominal model in Tab.I.

In the Heavy Payload scenario, we set $\theta_{\mathrm{s}} = 0.523$rad for both joints, that leads to a joint stiffness equal to $\sigma = 5.04$Nm/rad in case of zero deflection. Analogously, in the Light Payload scenario, we set $\theta_{\mathrm{s}} = 0.349$rad leading to $\sigma = 1.57$Nm/rad in case of zero deflection. Additionally, both scenarios are performed using three trajectories: the sinusoidal (20) and the minimum jerk (21) with $t_{\mathrm{f}} = 10$s and $t_{\mathrm{f}} = 1$s.

Fig. 7, 8, and 9 show the results. Fig. 7(a), 8(a), and 9(a) reports the error. Fig. 7(b), 8(b), and 9(b) show the final output and Fig. 7(c), 8(c), and 9(c) depicts the final control action. Finally, Fig. 7(d), 8(d), and 9(d) show the final joints evolution.

Finally, Fig. 10 shows a photo-sequence of the $R\overline{R}$, Heavy Payload, executing (21) with $t_{\mathrm{f}} = 10$s (see Video extension).

### G. Simulation and Experimental Results: $R\overline{2}\overline{R}$

In this experiment, we employ the $R\overline{2}\overline{R}$ arm to validate the effectiveness of the method in presence of different joint stiffness, repetitive and nonrepetitive disturbances. For each scenario, the task is to follow the desired trajectories (20) and (21) with the output function (13). The starting configuration is $\bar{x}(0) = 0_{6\times1}$, which leads to $u_0 = 0 \in \mathbb{R}$. The learning gain is chosen as in GSP1, i.e., Corollary 2, using the nominal model in Tab. I with $S = [1, 0, 0]^{\top}$, $n = 3$, and $n_{\mathrm{a}} = 1$.

We test two stiffness configurations: Softer case obtained with $\theta_{\mathrm{s}} = 0.349$rad, which leads to $\sigma = 1.57$Nm/rad in case of zero deflection, and Stiffer case, with $\theta_{\mathrm{s}} = 0.523$rad and $\sigma = 5.04$Nm/rad in case of zero deflection. In the disturbed scenario, we attach a pendulum with a mass equal to 0.1kg to the tip of the robot (see Fig. 11). The mass is free to oscillate during the robot motion. Its dynamics is not modeled in (1), leading to a repetitive disturbance [45]. This experiment is called Pendulum, and it is a direct application of Remark 3. Additionally, we also test the iterative algorithm in the presence of nonrepetitive disturbances. In particular, every 5 iterations, the user hits the robot. These experiments reproduce the presence of the disturbances $v_j(t)$. We test this case in the Softer and Stiffer scenarios and follow the two desired trajectories, minimum jerk and sinusoidal, respectively. Fig. 12 and 13 compare the simulation and the experimental results for (20) and (21), respectively. Fig. 12(a) and 13(a) report the error, while Fig. 12(b) and 13(b) show the final output. Fig. 13(c) and 12(c) depict the leaned control action. Fig. 11 depicts a photo-sequence of the Pendulum scenario executing (20) at the last iteration (see Video extension).

### H. Simulation and Experimental Results: $R\overline{R}R\overline{R}$

This experiment aims at validating the proposed approach with a MIMO system, varying also the passive joint stiffness. We here report the results of the $R\overline{R}R\overline{R}$ robot, whose dynamic parameters are listed in Tab. I. The selection matrix $S \in \mathbb{R}^{n\times n_{\mathrm{a}}}$, with $n = 4$ and $n_{\mathrm{a}} = 2$, is a null matrix except for $S_{1,1} = S_{3,2} =$

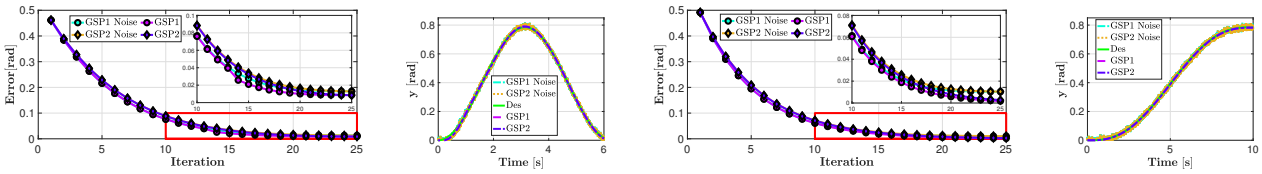


(a) Error evolution over iteration. (b) Output evolution. (c) Error evolution over iteration. (d) Output evolution.

Fig. 5. $R\overline{9R}$: simulation results for the sinusoidal trajectory ((a),(b)) and for the minimum jerk trajectory ((c)-(d)). Different conditions have been tested by varying the gains and the noise affecting the robot.

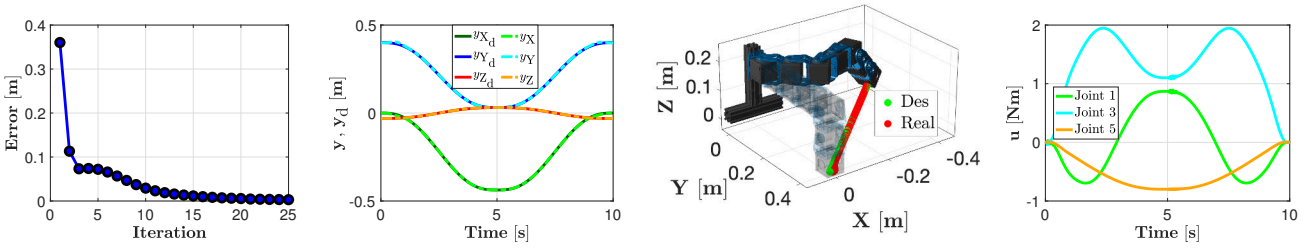


(a) Error evolution over iteration. (b) Output evolution over time. (c) Visualization output performance. (d) Final control action .

Fig. 6. $R\overline{R}\overline{R}R\overline{R}$: simulation results. In Fig. 6(c) the transparent structure depicts the initial and final robot configuration.

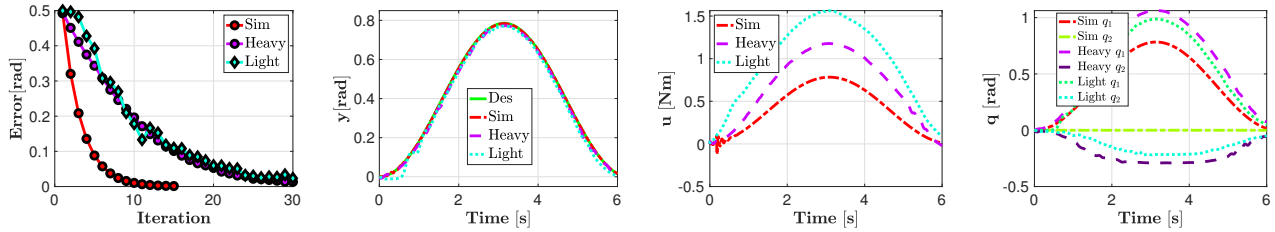


(a) Error evolution. (b) Output evolution. (c) Control action. (d) Joints evolution.

Fig. 7. $R\overline{R}$: results for the sinusoidal trajectory $t_f = 10$s. We vary joints stiffness and payload of the robot.

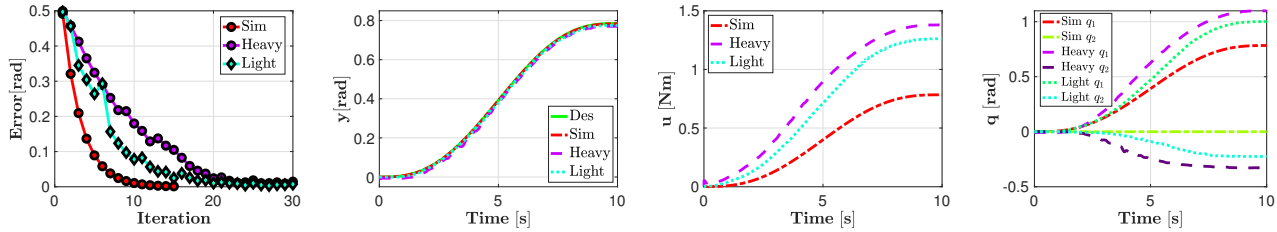


(a) Error evolution. (b) Output evolution. (c) Control action. (d) Joints evolution.

Fig. 8. $R\overline{R}$: results for the minimum jerk trajectory $t_f = 10$s. We vary joints stiffness and payload of the robot.

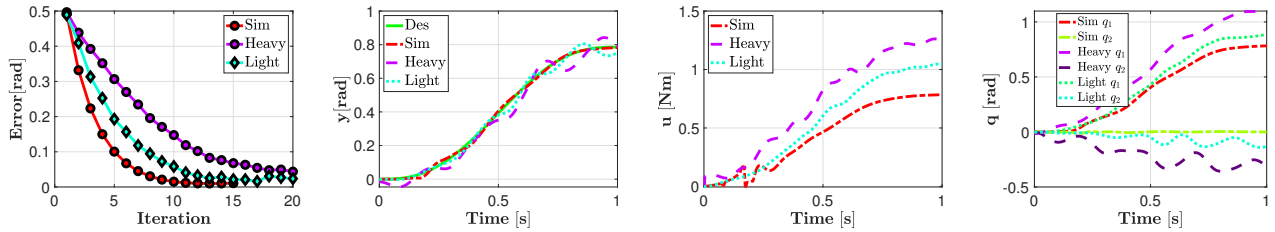


(a) Error evolution. (b) Output evolution. (c) Control action. (d) Joints evolution.

Fig. 9. $R\overline{R}$: results for the minimum jerk trajectory $t_f = 1$s. We vary joints stiffness and payload of the robot.

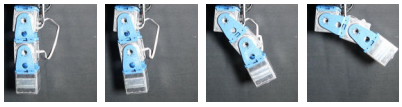

Fig. 10. $R\overline{R}$: photo-sequence of the final (21) with $t_f = 10$s, heavy payload.

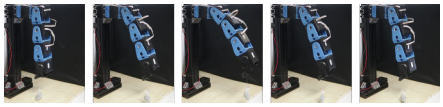

Fig. 11. $R\overline{2R}$: photo-sequence of the final (20), Pendulum.

1. The output function is (14), i.e., horizontal plane. We test two planar trajectories: Circumference and Planar Swing. Both tasks are performed in two configurations: Soft and Stiff. In particular, we vary the $\theta_s$ of the passive joints, which is set as $\theta_s = 0.349$rad and $\theta_s = 0.523$rad respectively. Conversely, the active ones have a fixed preset equal to $\theta_s = 0.698$rad, leading to $\sigma = 13.44$Nm/rad in case of zero deflection.

*1) Circumference:* The desired trajectory is a circumference (22) with $r_c = 50$mm and $t_f = 5$s. The chosen initial pose is $\bar{x}(0) = [0,\ 0,\ \pi/3,\ 0_{1\times5}]^\top$, hence, the initial guess is $u_0/K_{1,1} = [0,\ \pi/3]^\top$. We design the learning gain via GSP2.

Fig. 14 reports a photo-sequence of the Circumference trajectory final execution (see Video extension). Fig. 15 compares the results in both configurations. Fig. 15(a) reports the error evolution, while Fig. 15(c) shows the final output evolution. Fig. 15(b) depicts the learned control action.

*2) Planar Swing:* The robot swings from the initial Cartesian position $y_s = y(0) = [-0.27,\ 0.30]^\top$m to the final position $y_f = y(t_f) = [0.15,\ 0.38]^\top$m. Then, it swings back to the initial one, i.e., $y(2t_f) = y(0)$. The desired trajectory is composed of two minimum jerk signals (21), lasting $t_f =$ 5s each, so the task lasts 10s in total. The initial pose is $\bar{x}(0) = [\pi/6,\ 0,\ \pi/6,\ 0_{1\times5}]^\top$, hence, the initial guess is $u_0/K_{1,1} = [\pi/6,\ \pi/6]^\top$. We design the learning gain via GSP2.

Fig. 16 shows a photo-sequence of the Circumference trajectory execution at the last iteration (see Video extension). Fig. 17 compares the results in both configurations. Fig. 17(a) reports the error evolution, while Fig. 17(c) shows the final output evolution. Fig. 17(b) depicts the leaned control action.

## V. Discussion

In this section, we discuss the results of Sec. IV. We employed several different robotic structures varying the number of passive elements, payloads, desired trajectories, stiffness profiles, and disturbances.

The applicability of the iterative method is limited to intrinsically stable systems and the controller (5) cannot compensate for nonrepetitive disturbances in the time domain. This is true for all the pure feedforward approach. Conversely, Taking inspiration from, e.g., [23], [24], [42], it would be possible to include also a feedback loop in the control law. However, in this case, a different convergence condition is required.

We compared our iterative method with baseline controllers, namely PD and CT, Fig. 4. Since the initial guess is such that the system does not move, Fig. 4(a) shows that ILC has the worst performance at the first iterations.Refining the input, the ILC law achieves performance (RMS $\sim 10^{-4}$rad) that are comparable with the one of CT with perfect knowledge of the model (RMS $\sim 10^{-3}$rad), Fig. 4(b). In case of inaccurate model, the CT performance are drastically reduced. Conversely, the ILC continues to achieve analogous performance at the cost of a slower learning rate. PD shows always the worst performance.

The baseline controllers are feedback approaches, differently from the proposed ILC, which is purely feedforward. Thus, the performance of the CT and PD are obtained drastically altering the robot compliance. Additionally, classical model-based feedforward inverse dynamic controllers cannot be applied for highly underactuated systems, because they require information about the $x_d$, which cannot be obtained uniquely from $y_d$.

Regarding the ILC results, we note that, even though the model of the system is not accurate, the method improve the tracking performance within the iteration domain. In the simulations, the match between the model and the controlled system is perfect, and numerical issues in the derivatives estimation are not present, leading to a smooth error convergence. Conversely, the experiments present model and measurement inaccuracies. However, the obtained tracking error at the last iteration is comparable with the simulations at the cost of a greater number of trials, Fig.5(a),5(c),6(a),6(d),7(a),7(c)8(a),8(c),9(a),9(c),12(a),12(c), 13(a),13(c),15(a),15(b), and 17(a), 17(b).

Underactuated compliant arms usually present oscillatory movements. However, the method we proposed is able to achieve satisfying tracking performance at the last iteration Fig.5(b),5(d),6(b),7(b),8(b),9(b),12(b),13(b), 15(c), and 17(c). The only exception is (21) with $t_f = 1$s and heavy payload, depicted in Fig. 9. In this case the comparison between simulation and experiments empathizes that actuation saturation and errors in the derivatives prevent the oscillations removal, thus the performance are reduced.

The controller (5) can execute the task despite the presence of passive joints, unmodeled dynamics and disturbances while guaranteeing good tracking performances also varying payloads, stiffness profiles, and output functions. This happens also in the case of MIMO systems and systems with a number of unactuated joints that is even greater than the actuated ones. Fig. 7(d), 8(d), and 9(d) show the evolution of the joints in the $R\overline{R}$ experiments, proving that the unactuated joints present a not negligible motion. An analogous behavior occurs for all systems, but it is not reported here for the sake of space.

Sec. IV-G shows that the error convergence is (mostly) affected by the elastic behavior of the robot: softer behavior leads to slower learning processes Fig. 12(a)-13(a). Indeed, even though the final RMS error value is the same in both cases, the Stiffer robot reaches it about 5 iterations before the Softer one. Conversely, in Sec. IV-H, the absence of gravity lead to the same performances despite the variation of the stiffness profile, Fig. 15(a) and 17(a).

In Sec. IV-D, we point out that the convergence achieved with GSP1, i.e., (16), is faster than the one of GSP2, i.e., (18), at the cost of a more accurate description of the model. Indeed, if the robot model is available, the learning process can be expedited designing a learning gain such as in (16)-(17), and potentially using a model-based initial guess $u_0$. Conversely, if

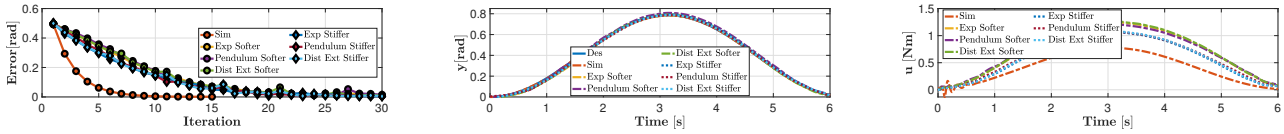


(a) Error evolution over iteration. (b) Output evolution over time. (c) Control action.

Fig. 12. $R\overline{2}\overline{R}$: simulation and experimental results for the sinusoidal trajectory. We vary the joints stiffness, we test the method in the case of disturbances.

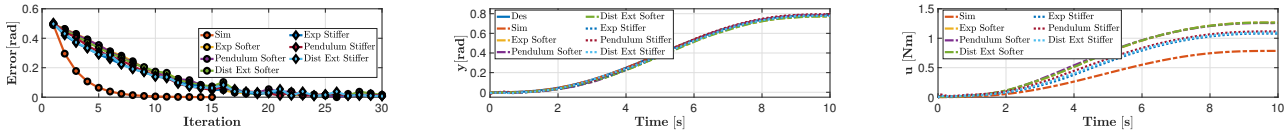


(a) Error evolution over iteration. (b) Output evolution over time. (c) Final control action.

Fig. 13. $R\overline{2}\overline{R}$: simulation and experimental results for the minimum jerk trajectory. We vary the joints stiffness, we test the method in the case of disturbances.

Fig. 14. $R\overline{R}R\overline{R}$: photo-sequence of the final Circumference task, Softer case.

the inertia matrix is not known, after the first iteration where the robot does not move, one checks the learning gain sign and properly select it in (18).

Additionally, according to Theorem 1, the presence of bounded nonrepetitive uncertainties in the output function leads to a bounded error: 0.01rad, which is achieved at iteration 20, Fig. 5(a) and 5(c). Moreover, the iterative framework can manage the presence of external disturbances of different types, namely Dist Ext and Pendulum scenario in Sec. IV-G. The former represents a nonrepetitive external disturbance on the robot, while the latter is an unmodeled dynamic effect. Indeed, Fig. 12-13 show that the iterative process learns the unmodeled dynamics of the mass and rejects the external disturbance reaching good tracking performances.

Finally, it is worth remarking that Proposition 1 holds true, then the relative degree $r$ is equal to $r=2$, so the convergence is guaranteed thanks to the choice of the gains.

## VI. Conclusion and Future Work

In this paper, we proposed a control framework to precisely follow a trajectory with underactuated compliant arms presenting any combination of active and passive elastic joints with no limitation on their number. For this scope, we designed a pure feedforward control framework based on the ILC approach. The convergence of the method is proved also in the presence of bounded disturbances. The applicability of the approach is guaranteed via inertial conditions on the system and output functions, and via design choices leading to stable behavior. Additionally, we proposed two automatic procedures to select the learning gains. Finally, we compared the method with SoA control algorithms and we extensively validate its effectiveness varying trajectories, the number of passive and active joints, stiffness, robots, output functions, disturbances, and payloads.

Future extensions of this work will apply the iterative control to a soft continuum robot [22].

## Appendix

***Proof of Theorem 1.*** To keep the notation simple, we will omit the time dependence. Given (5) and (6), one has

$$u_{\mathrm{d}}-u_{j+1}=\left(I_{n_{\mathrm{a}}}-\Gamma_j\Upsilon_r E(x_j)\right)\left(u_{\mathrm{d}}-u_j\right)-\Gamma_j\Phi(x_j,x_{\mathrm{d}}) +\Gamma_j\Upsilon_r\left(E(x_j)-E(x_{\mathrm{d}})\right)u_{\mathrm{d}}+\Gamma_j\sum_{s=0}^{r}\Upsilon_s w_j^{(s)}\,. \tag{25}$$

Given the definitions $\delta u_j \triangleq u_{\mathrm{d}}-u_j$ and $\delta x_j \triangleq x_{\mathrm{d}}-x_j$, we can write the following inequality

$$\left\|\delta u_{j+1}\right\| \le \left\|I_{n_{\mathrm{a}}}-\Gamma_j\Upsilon_r E(x_j)\right\|\left\|\delta u_j\right\|+\left\|\Gamma_j\right\|\left\|\Phi(x_j,x_{\mathrm{d}})\right\| +\left\|\Gamma_j\right\|\left\|\Upsilon_r\right\|\left\|E(x_j)-E(x_{\mathrm{d}})\right\|\left\|u_{\mathrm{d}}\right\|+\left\|\Gamma_j\right\|\bar{b}_{\mathrm{w}}\,, \tag{26}$$

where $\bar{b}_{\mathrm{w}} \ge (r+1)\max\{\|\Upsilon_0\|b_{\mathrm{w}},\cdots,\|\Upsilon_r\|b_{\mathrm{wr}}\}\ge 0$. Similarly, recalling assumptions A2, A3, and (6), we can compute a finite positive constant $\overline{\Phi}$ such that

$$\left\|\Phi(x_j,x_{\mathrm{d}})\right\| = \left\|\sum_{s=0}^{r}\Upsilon_s\left(L_f^s h(x_{\mathrm{d}})-L_f^s h(x_j)\right)\right\| \le \sum_{s=0}^{r}\left\|\Upsilon_s\Phi_s\right\|\left\|\delta x_j\right\| \le \overline{\Phi}\left\|\delta x_j\right\|\,, \tag{27}$$

where $\overline{\Phi}\ge(r+1)\max\{\|\Upsilon_0\Phi_0\|,\cdots,\|\Upsilon_r\Phi_r\|\}\ge 0$.

Let (7) be true, using (27) and recalling assumption A3, we can derive the following inequality

$$\left\|\delta u_{j+1}\right\| \le \rho\left\|\delta u_j\right\|+\left\|\Gamma_j\right\|\left(\left(\left\|\Upsilon_r\right\|\eta\left\|u_{\mathrm{d}}\right\|+\overline{\Phi}\right)\left\|\delta x_j\right\|+\bar{b}_{\mathrm{w}}\right)\,. \tag{28}$$

Defining $\mu \triangleq \sup_t\left\{\left\|\Gamma_j\right\|\left(\left\|\Upsilon_r\right\|\eta\left\|u_{\mathrm{d}}\right\|+\overline{\Phi}\right)\right\}$, we obtain

$$\left\|\delta u_{j+1}\right\| \le \rho\left\|\delta u_j\right\|+\mu\left\|\delta x_j\right\|+\left\|\Gamma_j\right\|\bar{b}_{\mathrm{w}}\,. \tag{29}$$

Given assumption A3 and the system (2), one has

$$\left\|\delta x_j\right\| \le b_{\mathrm{l}}+\int_0^t\left(f_0+g_0\left\|u_{\mathrm{d}}(z)\right\|\right)\left\|\delta x_j(z)\right\| +\left\|g(x_j(z))\right\|\left\|\delta u_j(z)\right\|+b_{\mathrm{v}}\mathrm{d}z\,. \tag{30}$$

Applying the Gronwall's Lemma to (30) leads to

$$\left\|\delta x_j\right\| \le b_{\mathrm{l}}\mathrm{e}^{c_2 t}+\int_0^t\left(c_1\left\|\delta u_j(z)\right\|+b_{\mathrm{v}}\right)\mathrm{e}^{c_2(t-z)}\mathrm{d}z\,, \tag{31}$$

where, $c_2 \triangleq \sup_t\{f_0+g_0\|u_{\mathrm{d}}\|\}$ and $c_1 \triangleq \sup_t\left\{\left\|g(x_j)\right\|\right\}$. Substituting (31) into (29) leads to

$$\left\|\delta u_{j+1}\right\| \le \rho\left\|\delta u_j\right\|+\mu b_{\mathrm{l}}\mathrm{e}^{c_2 t}+\left\|\Gamma_j\right\|\bar{b}_{\mathrm{w}} +\mu\int_0^t\left(c_1\left\|\delta u_j(z)\right\|+b_{\mathrm{v}}\right)\mathrm{e}^{c_2(t-z)}\mathrm{d}z\,. \tag{32}$$

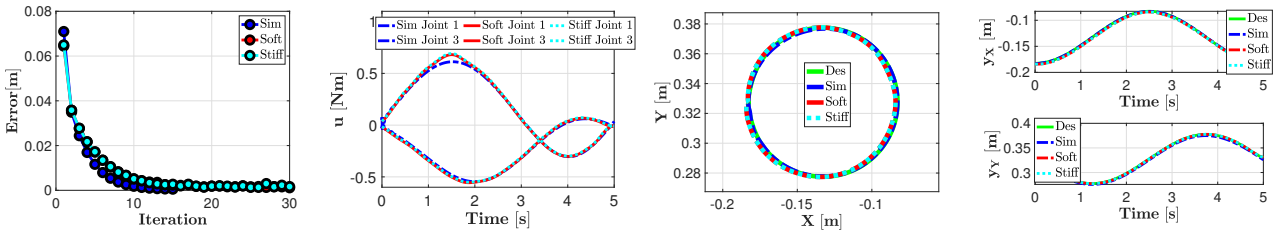


(a) Error evolution over iteration. (b) Control action. (c) Output evolution over time in the horizontal plane.

Fig. 15. $R\bar{R}R\bar{R}$: experimental results for the planar Circumference. Different conditions have been tested by varying the stiffness of the passive joints.

Fig. 16. $R\bar{R}R\bar{R}$: photo-sequence of the final Swing task, Softer case.

Computing the $\lambda-$norm of (32) leads to

$$\begin{aligned}\left|\left|\delta u_{j+1}\right|\right|_\lambda &\leq \rho\left|\left|\delta u_j\right|\right|_\lambda + \mu b_\mathrm{l} \sup_t\left\{\mathrm{e}^{(c_2-\lambda)t}\right\} + \left|\left|\Gamma_j\right|\right|_\lambda \bar{b}_\mathrm{w} \\ &+ \sup_t\left\{\int_0^t \mathrm{e}^{(c_2-\lambda)(t-z)}\mathrm{d}z\right\}\mu\left(c_1\left|\left|\delta u_j\right|\right|_\lambda + b_\mathrm{v}\right) .\end{aligned} \tag{33}$$

Solving the integral in (33) and defining $\bar{b}_j \triangleq \mu b_\mathrm{l} + \left|\left|\Gamma_j\right|\right|_\lambda \bar{b}_\mathrm{w} + \mu b_\mathrm{v}\left(1-\mathrm{e}^{(c_2-\lambda)t_\mathrm{f}}\right)/\left(\lambda-c_2\right)$ lead to

$$\left|\left|\delta u_{j+1}\right|\right|_\lambda \leq \left(\rho + \frac{\mu c_1\left(1-\mathrm{e}^{(c_2-\lambda)t_\mathrm{f}}\right)}{\lambda-c_2}\right)\left|\left|\delta u_j\right|\right|_\lambda + \bar{b}_j . \tag{34}$$

Defining $\zeta(\lambda) \triangleq \left(1-\mathrm{e}^{(c_2-\lambda)t_\mathrm{f}}\right)/\left(\lambda-c_2\right)$, we compact (34) as $\left|\left|\delta u_{j+1}\right|\right|_\lambda \leq \left(\rho+\mu\zeta(\lambda)\right)\left|\left|\delta u_j\right|\right|_\lambda + \bar{b}_j = \overline{\rho}\left|\left|\delta u_j\right|\right|_\lambda + \bar{b}_j$.

For hypotheses $\rho < 1$, then $\forall c_2$, $\exists\lambda$ large enough such that $\overline{\rho} < 1$. Hence, defining $\bar{b} = \max_j \bar{b}_j$, and substituting the previous $j$ trials, we have

$$\left|\left|\delta u_{j+1}\right|\right|_\lambda \leq \overline{\rho}^j\left|\left|\delta u_0\right|\right|_\lambda + \bar{b}\frac{1-\overline{\rho}^{j-1}}{1-\overline{\rho}} . \tag{35}$$

Then, when the index $j$ approaches $+\infty$, we have

$$\lim_{j\to+\infty}\left|\left|\delta u_{j+1}\right|\right|_\lambda \leq \bar{b}/\left(1-\overline{\rho}\right) \triangleq b_\mathrm{u} . \tag{36}$$

This proves (8).

Recalling (31) and computing its $\lambda$-norm, we obtain

$$\left|\left|\delta x_j\right|\right|_\lambda \leq b_\mathrm{l} + \left(c_1\left|\left|\delta u_j\right|\right|_\lambda + b_\mathrm{v}\right)\zeta(\lambda) . \tag{37}$$

Computing the limit and recalling (36), we have

$$\lim_{j\to+\infty}\left|\left|\delta x_j\right|\right|_\lambda \leq b_\mathrm{l} + \left(c_1 b_\mathrm{u} + b_\mathrm{v}\right)\zeta(\lambda) \triangleq b_\mathrm{x} . \tag{38}$$

This proves (9).

To prove (10), we start by noting that if (7) is satisfied, then $\Gamma_j$ is full rank. This can be easily proven by contradiction. Let us suppose that (7) is satisfied and $\Gamma_j$ singular. This implies that the spectral radius of $I_{n_\mathrm{a}} - \Gamma_j(t)\Upsilon_r E(x_j)$ is (greater or) equal to 1. Recalling that the spectral radius of a matrix is always lesser or equal to any natural norm of the same matrix (see, e.g., Chap. 10 of [46]), we have that this contradicts the validity of (7), which is absurd. Inverting $\Gamma_j$ in (5) and recalling (A1), we have ${}^r e_j = \Gamma_j^{-1}\left(u_{j+1}-u_j\right) = \Gamma_j^{-1}\left(\delta u_{j+1} - \delta u_j\right)$. Computing its $\lambda$-norm, we can write

$$\left|\left|{}^r e_j\right|\right|_\lambda \leq \left|\left|\Gamma_j^{-1}\right|\right|_\lambda\left(\left|\left|\delta u_{j+1}\right|\right|_\lambda + \left|\left|\delta u_j\right|\right|_\lambda\right) . \tag{39}$$

We define $b_\gamma \triangleq \max_j\left|\left|\Gamma_j^{-1}\right|\right|_\lambda$. Then, computing the limit of (39) and recalling (36), we have

$$\lim_{j\to+\infty}\left|\left|{}^r e_j\right|\right|_\lambda \leq 2 b_\gamma b_\mathrm{u} \triangleq b_\mathrm{e} . \tag{40}$$

This proves (10), and it concludes the proof of Theorem 1. □

***Proof of Corollary 1.*** If $l_j \equiv 0$, $v_j(t) \equiv 0$, and $w_j(t) \equiv 0$, then $\bar{b}$ in (36) is equal to 0, i.e., perfect convergence in (8). Then, it comes that (38) and (40) are 0. This concludes the proof. □

***Proof of Proposition 1.*** Differentiating $h(q,\dot{q}) \in \mathbb{R}^{n_\mathrm{a}}$ leads to

$$\dot{y} = \frac{\partial h(q,\dot{q})}{\partial q}\dot{q} + \frac{\partial h(q,\dot{q})}{\partial \dot{q}}\ddot{q} = L_f h(q,\dot{q}) + E(q)u . \tag{41}$$

Directly substituting (4) in (41) yields to

$$\begin{aligned}L_f h(q,\dot{q}) &= \frac{\partial h(q,\dot{q})}{\partial q}\dot{q} - \frac{\partial h(q,\dot{q})}{\partial q}M^{-1}(q)N(q,\dot{q}) , \\ E(q,\dot{q}) &= \left(\partial h(q,\dot{q})/\partial q\right)M^{-1}(q)S ,\end{aligned} \tag{42}$$

which leads to (11).

Conversely, if $y = h(q) \in \mathbb{R}^{n_\mathrm{a}}$ then, $E(q,\dot{q})$ in (41) has not maximum rank. Differentiating the output function leads to

$$\begin{aligned}\ddot{y} &= \frac{\partial L_f h(q,\dot{q})}{\partial q}\dot{q} + \frac{\partial L_f h(q,\dot{q})}{\partial \dot{q}}\ddot{q} = L_f^2 h(q,\dot{q}) + E(q,\dot{q})u , \\ E(q,\dot{q}) &= \left(\partial L_f h(q,\dot{q})/\partial q\right)M^{-1}(q)S , \\ L_f^2 h(q,\dot{q}) &= \left(\partial L_f h(q,\dot{q})/\partial q\right)\dot{q} - \left(\partial L_f h(q,\dot{q})/\partial \dot{q}\right)N(q,\dot{q}) .\end{aligned} \tag{43}$$

This proof is completed. □

***Proof of Corollary 2.*** The proof naturally comes from Proposition 1, and substituting (16) into (7). □

***Proof of Corollary 3.*** Let be $p \in [1\,,\,n_\mathrm{a}]$ the norm$-1$ index. Directly substituting (18) into the condition (7), one has

$$\sum_{i=1}^{n_\mathrm{a}}\left|1-\Gamma_{p,i}\Upsilon_{r_{p,p}}E_{p,i}(x)\right| = \sum_{i=1}^{n_\mathrm{a}}\left|1-\frac{E_{p,i}(x)}{\omega}\right| \leq \left|1-n_\mathrm{a}\left(\frac{\overline{E}}{\omega}\right)^{n_\mathrm{a}}\right| < 1 , \tag{44}$$

where $\overline{E} = \max_{i=1,\ldots,n_\mathrm{a}}\left\{E_{p,i}(x)\right\}$, $\forall x \in \mathbb{R}^{2n}$. Thus, $\exists\omega$ such that $\overline{E}/\omega$ is small by hypotheses, and (7) holds true. □

## References


[1] A. Albu-Schaffer, O. Eiberger, M. Grebenstein, S. Haddadin, C. Ott, T. Wimbock, S. Wolf, and G. Hirzinger, "Soft robotics," *IEEE Robotics & Automation Magazine*, vol. 15, no. 3, pp. 20–30, 2008.

[2] B. Vanderborght, A. Albu-Schäffer, A. Bicchi, E. Burdet, D. G. Caldwell, R. Carloni, M. Catalano, O. Eiberger, W. Friedl, G. Ganesh *et al.*, "Variable impedance actuators: A review," *Robotics and autonomous systems*, vol. 61, no. 12, pp. 1601–1614, 2013.

[3] C. Della Santina, "Flexible manipulators," *Encyclopedia of Robotics*, 2021.

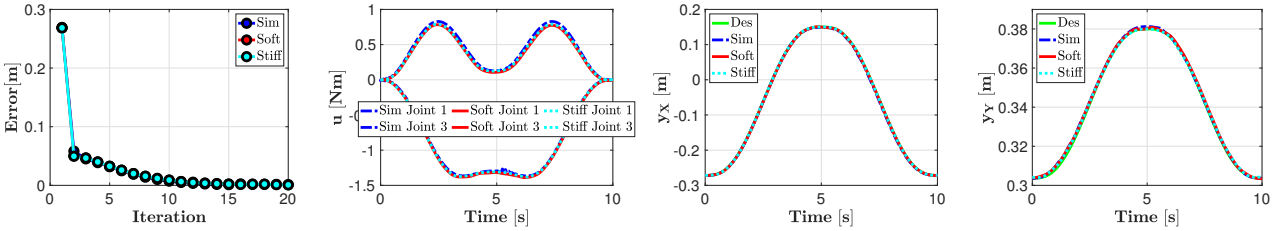


(a) Error evolution over iteration. (b) Control action. (c) Output evolution over time in the horizontal plane.

Fig. 17. $R\bar{R}R\bar{R}$: experimental results for the planar Swing. Different conditions have been tested by varying the stiffness of the passive joints.


[4] D. Rus and M. T. Tolley, "Design, fabrication and control of soft robots," *Nature*, vol. 521, no. 7553, pp. 467–475, 2015.

[5] F. Angelini, C. Petrocelli, M. G. Catalano, M. Garabini, G. Grioli, and A. Bicchi, "Softhandler: An integrated soft robotic system for handling heterogeneous objects," *IEEE Robotics & Automation Magazine*, vol. 27, no. 3, pp. 55–72, 2020.

[6] V. Etxebarria, A. Sanz, and I. Lizarraga, "Control of a lightweight flexible robotic arm using sliding modes," *International Journal of Advanced Robotic Systems*, vol. 2, no. 2, p. 11, 2005.

[7] S. Seok, C. D. Onal, K.-J. Cho, R. J. Wood, D. Rus, and S. Kim, "Meshworm: a peristaltic soft robot with antagonistic nickel titanium coil actuators," *IEEE/ASME Transactions on mechatronics*, vol. 18, no. 5, pp. 1485–1497, 2012.

[8] J. P. Vasconez, G. A. Kantor, and F. A. A. Cheein, "Human–robot interaction in agriculture: A survey and current challenges," *Biosystems engineering*, vol. 179, pp. 35–48, 2019.

[9] Z. Pang, G. Yang, R. Khedri, and Y.-T. Zhang, "Introduction to the special section: convergence of automation technology, biomedical engineering, and health informatics toward the healthcare 4.0," *IEEE Reviews in Biomedical Engineering*, vol. 11, pp. 249–259, 2018.

[10] M. Decker, M. Fischer, and I. Ott, "Service robotics and human labor: A first technology assessment of substitution and cooperation," *Robotics and Autonomous Systems*, vol. 87, pp. 348–354, 2017.

[11] C. Sampedro, A. Rodriguez-Ramos, H. Bavle, A. Carrio, P. de la Puente, and P. Campoy, "A fully-autonomous aerial robot for search and rescue applications in indoor environments using learning-based techniques," *Journal of Intelligent & Robotic Systems*, vol. 95, no. 2, pp. 601–627, 2019.

[12] J. E. Pratt and B. T. Krupp, "Series elastic actuators for legged robots," in *Unmanned Ground Vehicle Technology Vi*, vol. 5422. International Society for Optics and Photonics, 2004, pp. 135–144.

[13] S. D. Eppinger, W. P. Seering *et al.*, "Three dynamic problems in robot force control," *IEEE Transactions on Robotics and Automation*, vol. 8, no. 6, pp. 751–758, 1992.

[14] A. De Luca and P. Lucibello, "A general algorithm for dynamic feedback linearization of robots with elastic joints," in *Proceedings. 1998 IEEE International Conference on Robotics and Automation (Cat. No. 98CH36146)*, vol. 1. IEEE, 1998, pp. 504–510.

[15] P. Tomei, "A simple pd controller for robots with elastic joints," *IEEE Transactions on automatic control*, vol. 36, no. 10, pp. 1208–1213, 1991.

[16] M. Keppler, D. Lakatos, C. Ott, and A. Albu-Schäffer, "Elastic structure preserving (esp) control for compliantly actuated robots," *IEEE Transactions on Robotics*, vol. 34, no. 2, pp. 317–335, 2018.

[17] C. Della Santina, R. K. Katzschmann, A. Bicchi, and D. Rus, "Dynamic control of soft robots interacting with the environment," in *2018 IEEE International Conference on Soft Robotics (RoboSoft)*. IEEE, 2018, pp. 46–53.

[18] A. Palleschi, R. Mengacci, F. Angelini, D. Caporale, L. Pallottino, A. De Luca, and M. Garabini, "Time-optimal trajectory planning for flexible joint robots," *IEEE Robotics and Automation Letters*, vol. 5, no. 2, pp. 938–945, 2020.

[19] S. Tonkens, J. Lorenzetti, and M. Pavone, "Soft robot optimal control via blackuced order finite element models," in *2021 IEEE International Conference on Robotics and Automation (ICRA)*. IEEE, 2021, pp. 12 010–12 016.

[20] M. Stölzle and C. Della Santina, "Piston-driven pneumatically-actuated soft robots: modeling and backstepping control," *IEEE Control Systems Letters*, vol. 6, pp. 1837–1842, 2021.

[21] E. Franco and A. Garriga-Casanovas, "Energy-shaping control of soft continuum manipulators with in-plane disturbances," *The International Journal of Robotics Research*, vol. 40, no. 1, pp. 236–255, 2021.

[22] C. Della Santina, C. Duriez, and D. Rus, "Model based control of soft robots: A survey of the state of the art and open challenges," *arXiv preprint arXiv:2110.01358*, 2021.

[23] F. Angelini, C. Della Santina, M. Garabini, M. Bianchi, G. M. Gasparri, G. Grioli, M. G. Catalano, and A. Bicchi, "Decentralized trajectory tracking control for soft robots interacting with the environment," *IEEE Transactions on Robotics*, vol. 34, no. 4, pp. 924–935, 2018.

[24] R. Mengacci, F. Angelini, M. G. Catalano, G. Grioli, A. Bicchi, and M. Garabini, "On the motion/stiffness decoupling property of articulated soft robots with application to model-free torque iterative learning control," *The International Journal of Robotics Research*, p. 0278364920943275, 2020.

[25] T. G. Thuruthel, E. Falotico, F. Renda, and C. Laschi, "Model-based reinforcement learning for closed-loop dynamic control of soft robotic manipulators," *IEEE Transactions on Robotics*, vol. 35, no. 1, pp. 124–134, 2018.

[26] O. Fischer, Y. Toshimitsu, A. Kazemipour, and R. K. Katzschmann, "Dynamic control of soft manipulators to perform real-world tasks," *arXiv preprint arXiv:2201.02151*, 2022.

[27] T. M. Bieze, F. Largilliere, A. Kruszewski, Z. Zhang, R. Merzouki, and C. Duriez, "Finite element method-based kinematics and closed-loop control of soft, continuum manipulators," *Soft robotics*, vol. 5, no. 3, pp. 348–364, 2018.

[28] M. W. Spong, "Partial feedback linearization of underactuated mechanical systems," in *Proceedings of IEEE/RSJ International Conference on Intelligent Robots and Systems (IROS'94)*, vol. 1. IEEE, 1994, pp. 314–321.

[29] D. Camilleri and T. Prescott, "Analysing the limitations of deep learning for developmental robotics," in *conference on Biomimetic and Biohybrid Systems*. Springer, 2017, pp. 86–94.

[30] Z. Q. Tang, H. L. Heung, K. Y. Tong, and Z. Li, "Model-based online learning and adaptive control for a "human-wearable soft robot" integrated system," *The International Journal of Robotics Research*, vol. 40, no. 1, pp. 256–276, 2021.

[31] D. Bristow, M. Tharayil, and A. Alleyne, "A survey of iterative learning control," *IEEE Control Systems Magazine*, vol. 26, no. 3, pp. 96–114, 2006.

[32] C. Della Santina, M. Bianchi, G. Grioli, F. Angelini, M. Catalano, M. Garabini, and A. Bicchi, "Controlling soft robots: balancing feedback and feedforward elements," *IEEE Robotics & Automation Magazine*, vol. 24, no. 3, pp. 75–83, 2017.

[33] M. Pierallini, F. Angelini, R. Mengacci, A. Palleschi, A. Bicchi, and M. Garabini, "Trajectory tracking of a one-link flexible arm via iterative learning control," in *2020 IEEE/RSJ International Conference on Intelligent Robots and Systems (IROS)*. IEEE, 2020, pp. 7579–7586.

[34] M. Hofer, L. Spannagl, and R. D'Andrea, "Iterative learning control for fast and accurate position tracking with an articulated soft robotic arm," in *2019 IEEE/RSJ International Conference on Intelligent Robots and Systems (IROS)*. IEEE, 2019, pp. 6602–6607.

[35] D. Meng and K. L. Moore, "Robust iterative learning control for non-repetitive uncertain systems," *IEEE Transactions on Automatic Control*, vol. 62, no. 2, pp. 907–913, 2016.

[36] D. Meng, "Convergence conditions for solving robust iterative learning control problems under nonrepetitive model uncertainties," *IEEE transactions on neural networks and learning systems*, vol. 30, no. 6, pp. 1908–1919, 2018.

[37] D. Meng and J. Zhang, "Robust tracking of nonrepetitive learning control systems with iteration-dependent references," *IEEE Transactions on Systems, Man, and Cybernetics: Systems*, 2018.

[38] J. Zhang and D. Meng, "Convergence analysis of saturated iterative learning control systems with locally lipschitz nonlinearities," *IEEE*

*transactions on neural networks and learning systems*, vol. 31, no. 10, pp. 4025–4035, 2019.
[39] H.-S. Ahn, C.-H. Choi, and K.-b. Kim, "Iterative learning control for a class of nonlinear systems," *Automatica*, vol. 29, no. 6, pp. 1575–1578, 1993.
[40] A. Isidori, "Elementary theory of nonlinear feedback for multi-input multi-output systems," in *Nonlinear Control Systems*. Springer, 1995, pp. 219–291.
[41] C. Della Santina, "The soft inverted pendulum with affine curvature," in *2020 59th IEEE Conference on Decision and Control (CDC)*. IEEE, 2020, pp. 4135–4142.
[42] M. Pierallini, F. Angelini, A. Bicchi, and M. Garabini, "Swing-up of underactuated compliant arms via iterative learning control," *IEEE Robotics and Automation Letters*, vol. 7, no. 2, pp. 3186–3193, 2022.
[43] R. Mengacci, M. Garabini, G. Grioli, M. Catalano, and A. Bicchi, "Overcoming the torque/stiffness range tradeoff in antagonistic variable stiffness actuators," *IEEE/ASME Transactions on Mechatronics*, 2021.
[44] A. De Luca and G. Oriolo, "Trajectory planning and control for planar robots with passive last joint," *The International Journal of Robotics Research*, vol. 21, no. 5-6, pp. 575–590, 2002.
[45] M. Pierallini, F. Angelini, R. Mengacci, A. Palleschi, A. Bicchi, and M. Garabini, "A robust iterative learning control for continuous-time nonlinear systems with disturbances," *IEEE Access*, vol. 9, pp. 147 471–147 480, 2021.
[46] K. B. Petersen and M. S. Pedersen, "The matrix cookbook," nov 2012.

**Michele Pierallini** received the B.S. degree in biomedical engineering in 2017 and M.S. degree (cum laude) in automation and robotics engineering in 2020 from the University of Pisa, Pisa, Italy, where he is currently working toward the Ph.D. degree in robotics at the Research Center "Enrico Piaggio." His current research focuses on the control of soft robotic systems and iterative learning control.

**Franco Angelini** (Member, IEEE) received the B.S. degree in computer engineering in 2013 and M.S. degree (cum laude) in automation and robotics engineering in 2016 from the University of Pisa, Pisa, Italy. University of Pisa granted him also a Ph.D. degree (cum laude) in robotics in 2020 for which he was awarded with the 2021 SIDRA Award for the best PhD Theses in the area of Systems and Control Engineering at an Italian University. Franco is currently an Assistant Professor at University of Pisa. His main research interests are control of soft robotic systems, impedance planning, and robotic environmental monitoring.

**Riccardo Mengacci** received a Bachelor's Degree in Informatics and Automation Engineer from the Polytechnic University of Marche, Ancona in 2013 and a Master's Degree in Automation and Robotics Engineering from the University of Pisa in 2017. In 2021, he got his Ph.D. degree in robotics (cum laude) from the University of Pisa. His research activity focuses on design and control strategies for robotics applications.

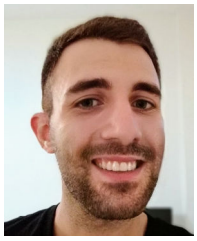

**Alessandro Palleschi** is currently a Ph.D. student in Smart Industry at the University of Pisa and at the Research Center "E. Piaggio". Born in Pisa, he received his BSc. in Electronic Engineering at the University of Pisa in 2015, and his MSc. in Robotics and Automation Engineering at the same institution in 2018, both cum laude. As a Ph.D. student, his research interests include Planning for Robotics Manipulation and Grasping with application to Logistics and Industry 4.0.

**Antonio Bicchi** is a scientist interested in robotics and intelligent machines. He holds a chair in Robotics at the University of Pisa, leads the Soft Robotics Laboratory at the Italian Institute of Technology in Genova, and is and Adjunct Professor at Arizona State University. His work has been recognized with many international awards and has earned him four prestigious grants from the European Research Council (ERC). He launched initiatives such as the WorldHaptics conference series, the IEEE Robotics and Automation Letters, and the Italian Institute of Robotics and Intelligent Machines.

**Manolo Garabini** graduated in Mechanical Engineering and received the Ph.D. in Robotics from the University of Pisa where he is currently employed as Assistant Professor. His main research interests include the design, planning, and control of soft adaptive robots. He contributed to the realization of modular Variable Stiffness Actuators, to the design of the humanoid robot WALK-MAN and, to the development of efficient and effective compliance planning algorithms for interaction under uncertainties. Currently, he is the Principal Investigator in the THING H2020 EU Research Project for the University of Pisa, and the coordinator of the Dysturbance H2020 Eurobench sub-project. Finally, he is the coordinator of the H2020 EU Research Project Natural Intelligence.